Estimation of a source term in a two-dimensional heat transfer problem: application to an electron beam welding, theoretical and experimental validations

J. Guo, P. Le Masson, Sebastien Rouquette, Tahar Loulou, E. Artioukhine

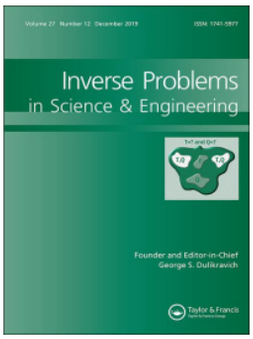

Inverse Problems in Science and Engineering

ISSN: 1741-5977 (Print) 1741-5985 (Online) Journal homepage: www.tandfonline.com/journals/gipe20

Estimation of a source term in a two-dimensional heat transfer problem: application to an electron beam welding, theoretical and experimental validations

J. Guo, P. Le Masson, S. Rouquette, T. Loulou & E. Artioukhine

To cite this article: J. Guo, P. Le Masson, S. Rouquette, T. Loulou & E. Artioukhine (2007) Estimation of a source term in a two-dimensional heat transfer problem: application to an electron beam welding, theoretical and experimental validations, Inverse Problems in Science and Engineering, 15:7, 743-763, DOI: 10.1080/17415970701198688

To link to this article: https://doi.org/10.1080/17415970701198688

Published online: 28 Sep 2007.

Inverse Problems in Science and Engineering
Vol. 15, No. 7, October 2007, 743–763

Taylor & Francis
Taylor & Francis Group

Estimation of a source term in a two-dimensional heat transfer problem: application to an electron beam welding, theoretical and experimental validations

J. GUO†, P. LE MASSON*†, S. ROUQUETTE‡,
T. LOULOU† and E. ARTIOUKHINE§

†LET2E/ETM: Laboratoire d'Etudes Thermique Energétique
et Environnement/Equipe Thermophysique et Matériaux, Université de Bretagne Sud,
C.U.R.S.T., Rue de Saint Maudé, F-56321 Lorient Cedex, France
‡Laboratoire des Systèmes Mécaniques et Ingénierie Simultanée (LASMIS),
Université de Technologie de Troyes – FRE CNRS 2719 –
12 Rue Marie Curie – 10010 TROYES Cedex, France
§Laboratoire CREST, UMR CNRS 6000, Université de Franche-Comté –
Université de Technologie de Belfort-Montbéliard, Site IGE,
2 avenue Jean Moulin, 90000 Belfort, France

(*Received 17 December 2005; revised 6 April 2006; in final form 8 June 2006*)

This article is concerned with the estimation of a heat source applied in the electron beam welding process by using temperature measurements in solid phase. The aim is to identify the energy distribution which is applied in the liquid and vapour zones. This identification is realized at each time in a transversal plan perpendicularly to the welding axis. For this work, the goals are, first, to analyse the feasibility of the estimation and, second, to estimate the energy distribution in a real case. The thermometallurgical model does not take into account the convective phenomena in the fused zone. We show the development of the experimentation, its realization and the exploitation of measurements. At last, the iterative regularization method and the measurements will be used for this two-dimensional metallurgical inverse heat transfer problem.

Keywords: Inverse thermal problem; Electron beam welding; Heat Affected Zone (HAZ); Thermocouple

1. Introduction

Welding is an assembling operation which affects both mechanical and structural properties and which is very sensitive to control parameters of technological processes. The first stage of this study is to choose these parameters which lead to an acceptable welding quality. The main difficulty of the theoretical analysis is that the exact

*Corresponding author. Email: philippe.le-masson@univ-ubs.fr

Inverse Problems in Science and Engineering
ISSN 1741-5977 print/ISSN 1741-5985 online © 2007 Taylor & Francis
http://www.tandf.co.uk/journals
DOI: 10.1080/17415970701198688

distribution of the thermal energy absorbed and generated in the liquid and vapour zones is not easy to predict and cannot be measured directly. When studying the welding, the theoretical analysis use complementary experimental information: the temperature measurements near the liquid zone and the microstructural properties (hardness, optical micrograph, etc.). The objective of this work is the estimation of the energy distribution in the welding zone. The temperature difference between the welding and solid zones is big enough, but there is a strong damping effect in the solid zone. That is why it is difficult to estimate correctly the energy distribution from the temperature measurements taken at points which are too far from the welding zone. Many works deal with the estimation of boundary conditions or the determination of distributed heat flux on the boundary of the body [1–3]. Few of these works consider experimental situations involving unknown heat sources. Silva Neto *et al*. [4] used the conjugate gradient algorithm to estimate the time-varying strength of a line source placed in a rectangular region with insulated boundaries, but the location of the source was specified. Le Niliot [5] studied linear inverse problems with two point heat sources, and experimental results were presented in [6].

In many studies, the inverse fusion and solidification problem has been analysed using a simplified approach based on only a conduction model in the liquid and vapor zones. Under these assumptions, 1D or 2D Stefan problems taking into account only the conduction effects in all the phases during the process were considered. The objective was to estimate an energy distribution [3], or a motion of the solid–liquid interface [7–10]. Another approach was to take into account the convection effects describing the Navier–Stokes equations in the liquid and vapor zones [11]. Mixed approaches were employed, in which an apparent source term is determined in the liquid and vapor zones representing the different phenomena [12]. At last, we can find applications which use the inverse technique and Bézier splines for identifying the location of the liquid–solid interface by solving an inverse geometry problem [13].

In this article, we use the first hypothesis for the electron beam welding process. We consider only the conduction effects for all phases (solid, liquid, and vapour). The iterative regularization method [2] is used to estimate the dissipation energy in the liquid and vapour zones. First, we present the electron beam welding technique and the used steel sample. Second, we describe the direct problem including the simulation of phase transformations and the source term (electron beam). Third, the estimation procedure is described. Fourth, the feasibility of the estimation is analyzed. Finally, the experimentation and the estimation results are discussed.

2. The electron beam welding

2.1. *Principle*

The electron beam (EB) welding is an assembling process in vacuum using a high density energy beam. This technique permits the welding of the high thicknesses (up to 16 cm) with a low width and a narrow Heat Affected Zone (HAZ). At the beginning of the welding process, the high power density of the EB leads to an evaporation of the material and then to a keyhole (figure 1). It is this keyhole and its displacement which generate the welded joint. The high penetration capacity of the beam with a narrow fusion zone characterizes the EB welding in comparison with

other weld methods. For these other methods, the penetration is limited by the heat conduction [14].

For this study, weld joints are used which are realized in the "Direction des Constructions Navales" (DCN) in Indret (44-France) (power of this EB: 100 kW). The welds are made of 18MnNiMo five steel samples (ASTM A508 Cl.3). In this article, a partial penetration welded joint is analysed. Figure 2 shows the micrography of this sample which is used to determine precisely the locations of the measurement points by using a scan of this welding joint. The high temperature level in the fusion and vapour zones prevents the installation of the thermocouples in these zones. The used thermocouples are thus located in the HAZ ($750°C < T < 1450°C$).The welding parameters are: voltage: $U = 60\,kV$, current $I = 0.29A$, velocity $v = 2.5\,mm\,s^{-1}$, focus current $I_f = 2.46A$.

With the experimental temperatures obtained from the thermocouples and corresponding diagrams (CCT or TTT) we will validate the simulation of the metallurgical transformations by comparing the experimental and simulated thermal and metallurgical parameters. Furthermore, temperatures computed at the

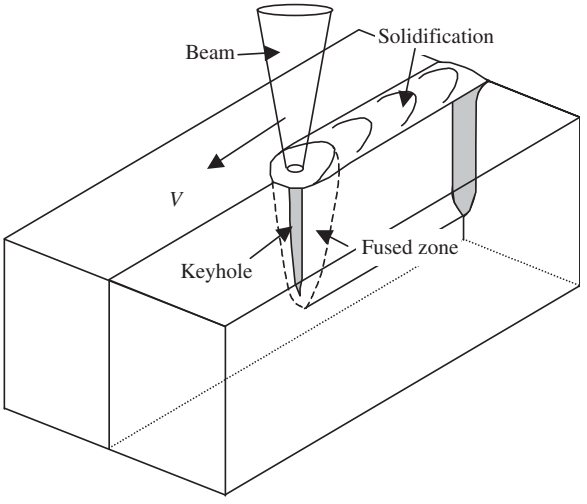

Figure 1. Welding process.

Figure 2. Weld joint.

thermocouple locations by solving the direct problem will be used to estimate the source term in the fusion and vapour zones.

2.2. *Numerical simulation of the electron beam welding*

Several works are concerned with the numerical simulation of the EB welding in the laboratory LET2E [15–17]. In these works, the SYSWELD code [18] was used. In this study, we use a new code analogous to SYSWELD which is incorporated in the developed estimation code. The finite difference method based on an implicit scheme is used to solve the direct and inverse problems. The equations are the heat conduction equation (1) and the metallurgical kinetic equations (2) of the type Leblond and Devaux [19] and Koistinen and Marburger [20]. The studied domain is one half of the transversal plane taken perpendicularly to the welding axis (figure 3).

$$\rho(T)C_p(T)\frac{\partial T}{\partial t} = \frac{\partial}{\partial x}\left(\lambda(T)\frac{\partial T}{\partial x}\right) + \frac{\partial}{\partial z}\left(\lambda(T)\frac{\partial T}{\partial z}\right) + \frac{\partial P_\alpha}{\partial t}L_{\alpha\gamma}(T) - \frac{\partial(\rho H)}{\partial t} + S(x,z,t) \tag{1}$$

$$\frac{\partial P}{\partial t} = \frac{P_{\text{eq}} - P}{\tau} f\left(\frac{\partial T}{\partial t}\right) \quad \text{and} \quad P = P_{\max}(1 - \exp(-b(T - M_s))) \tag{2}$$

The boundary and initial conditions are the following: at the lower, upper, and lateral surfaces, only the radiative conditions are fixed because the welding process is carried out in vacuum. For example, at the lower surface, the boundary condition is:

$$-\lambda(T)\frac{\partial T(x, z=0, t)}{\partial z} = \varepsilon\sigma\left[T^4(x, z=0, t) - T_{\text{inf}}^4\right] \tag{3}$$

On the axis:

$$\frac{\partial T(x=0, z, t)}{\partial x} = 0 \tag{4}$$

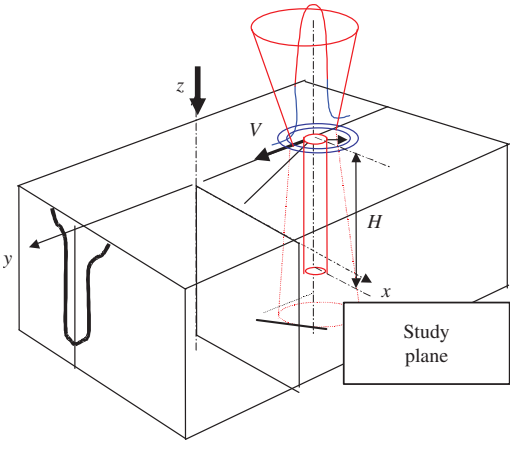

Figure 3. Definition of the study plane.

Initial conditions:

$$T(x,z,0) = T_0\,; P_\alpha(x,z,0) = 1 \tag{5}$$

In the heat conduction equation (1), the source terms $(\partial P_\alpha/\partial t)L_{\alpha\gamma}(T)$ and $(\partial(\rho H)/\partial t)$ allow to take into account the phase change enthalpy according to the temperature of the sample (metallurgical transformations for the first term – P_α is the proportion of metallurgic phase α, fusion and evaporation for the second). The transformation energy is calculated according to the phase enthalpy: $L_{\alpha\gamma}(T) = \rho_\gamma H_\gamma - \rho_\alpha H_\alpha$ and by considering two metallurgical phases only: γ(austenite) and α (ferrite, perlite, bainite, or martensite). The enthalpies of the phases α and γ are computed with the use of polynomial functions between 100°C and 1450°C. The parameters of the metallurgical kinetic equations are calculated by simulating the CCT diagram (figure 4).

For each time and space node, the cooling speed and the temperature value are used. With this information, the percentage P_i of the metallurgical transformation is computed. Moreover, the thermophysical characteristics $\rho(T)$, $C(T)$ and $\lambda(T)$ are calculated at all time steps by a law of mixtures according to the temperature, e.g., $\lambda(T) = P^*_\gamma\lambda_\gamma(T) + P^*_\alpha\lambda_\alpha(T) = \sum_i P_i\lambda_i(T)$.

For the phase γ and for $T < 145$°C:

$$\begin{aligned}\rho_\gamma C_\gamma(T) &= 3641440 + 4638.78 * T - 11.7784 * T^2 \\ &\quad + 0.0155136 * T^3 - 9.29165E-6 * T^4 + 2.03093E-9 * T^5 \\ \lambda_\gamma(T) &= 0.0148939 + 1.24115E-5 * T - 7.74533E-10 * T^2 \\ &\quad + 8.11438E-13 * T^3\end{aligned}$$

For the phase α and for $T < 750$°C:

$$\begin{aligned}\rho_\alpha C_\alpha(T) &= 3620850 + 2955.1 * T - 7.52398 * T^2 \\ &\quad + 0.0249182 * T^3 - 1.68686E-5 * T^4 \\ \lambda_\alpha(T) &= 0.0525037 - 3.35115E-5 * T \\ &\quad + 1.76665E-8 * T^2 - 1.74307E-11 * T^3\end{aligned}$$

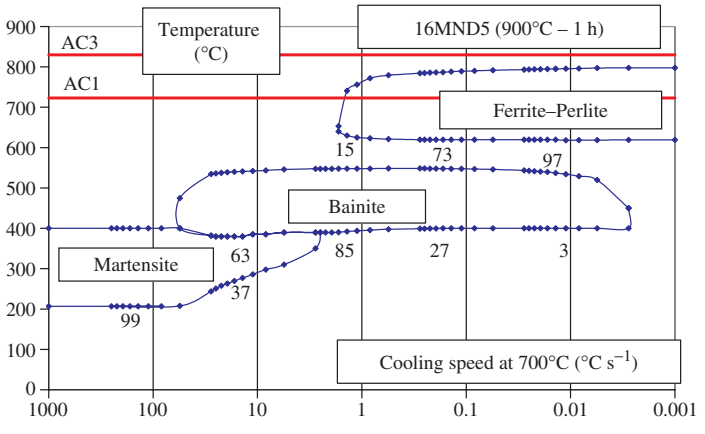

Figure 4. CCT diagram.

The other thermal transformations are computed between 1450°C and 1550°C for the fusion and between 2600°C and 2800°C for the evaporation. These enthalpies are given in Costantini's work [14]: $\Delta H_{fus} = 391970\,J\,kg^{-1}$ and $\Delta H_{vap} = 6332879\,J\,kg^{-1}$. At last, the thermophysical characteristics of the liquid and vapour phases are computed at the temperature 1450°C.

The initial data of the model is:
- The mesh;
- The thermophysical characteristics $\rho(T)$, $C(T)$, $\lambda(T)$ and $L_{\alpha\gamma}$ for the different phases according to the temperature;
- The initial and final temperatures of thermal transformations for all phases (CCT diagram);
- The initial temperature $T_0 = 20°C$ in whole domain;
- The ambient temperature T_{inf};
- The emissivity of the considered material is supposed to be constant and equal to 0.8.

The set of equations is solved with the use of a fine discretization of the domain near the EB zone (176 nodes in the vertical direction; 52 nodes in the transverse direction). The finite difference grid is uniform in the vertical direction, $\Delta z = 0.5\,mm$, and not uniform in the transverse direction, $0.05\,mm < \Delta x < 2\,mm$. The direct problem and the corresponding code have been verified in previous papers [15–17].

Figure 5 shows the comparison between the experimental data and numerical results for a Gaussian source [15]. Globally, we find a good level for the maximal temperatures. Some problems stay because we do not have the diffusion effect forward the beam. For this reason, it seems to be important to estimate, in this transversal plane, an apparent source term for modeling the diffusion effect in the steel.

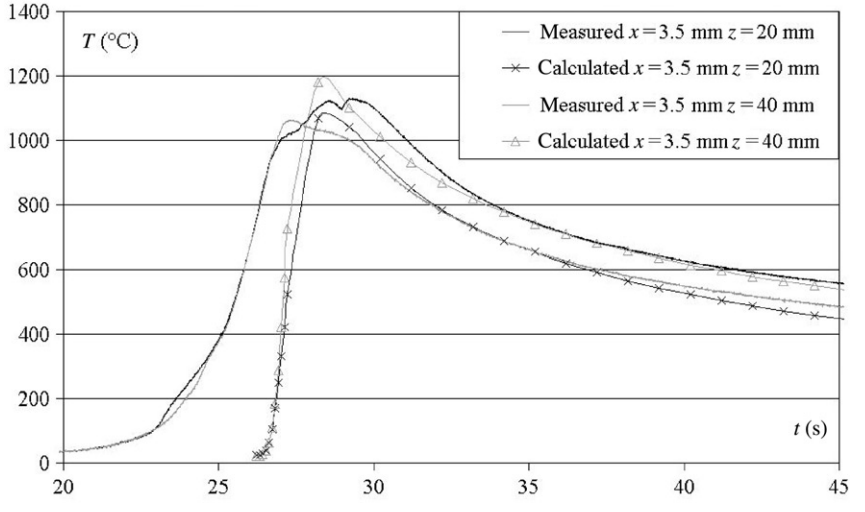

Figure 5. Comparison between the experimental and numerical temperatures.

3. Estimation algorithm

The objective of this research is to determine a source term $S(x, z, t)$. The determination is conducted from the temperature values measured in the heat affected zone at a distance between 2 mm and 8 mm from the welding axis. The time step used in the estimation is $\Delta t = 001$ s and the discretization on the welding axis is $\Delta z = 0.5$ mm and $\Delta x = 0.05$ mm.

3.1. *Minimization procedure*

The use of the iterative regularization method leads to the variational formulation of the inverse problem of estimating the source term and the residual functional minimization by utilizing the unconstrained conjugate gradient method. The residual functional is defined as:

$$J(S) = \frac{1}{2}\int_0^{t_f} \sum_{j=1}^{N} \left[T(x_j, z_j, t; S) - Y_j(t)\right]^2 \mathrm{d}t \tag{6}$$

where $T(x_j, z_j, t; S)$ and $Y_j(t)$ are the computed and measured temperature histories, respectively, at N various measurement points of the material. The inverse algorithm consists in minimizing this residual functional under constraints on the temperature given by the direct problem [equations (1) to (5)].

The function $S(z, x, t)$ is considered as an element of the Hilbert space L^2. The source term is computed as a grid function. In the iterative method, the desired function approximations are built at each iteration as follows:

$$S^{n+1} = S^n + \gamma^n D^n, \quad n = 1, \ldots, n^* \tag{7}$$

where n is the iteration index, n^* is the index of the last iteration, γ^n is the descent parameter, D^n is the descent direction given by:

$$D^{\mathrm{n}} = -\nabla J^n + \beta^n D^{n-1} \tag{8}$$

$$\text{where:} \quad \beta^n = \frac{\langle \nabla J^n - \nabla J^{n-1}, \nabla J^n \rangle}{(\nabla J^n)^2}, \ \beta^0 = 0. \tag{9}$$

$\langle , \rangle$ is the scalar product in Hilbert space L^2, S^0 is an initial approximation of the function to be estimated given *a priori*.

In the absence of noise, the iteration procedure is carried on until the following stopping criterion is verified:

$$\left|\frac{S^{n+1} - S^n}{S^n}\right| \leq \varepsilon_1 \tag{10}$$

The residual functional gradient ∇J^n is calculated at each computational grid node (x, z, t) by the following analytical relationship:

$$\nabla J^n = \psi(x, z, t) \tag{11}$$

where $\psi(x, z, t)$ is the solution of the adjoint problem [15] derived by using the approach given in [2].

$$-\rho C_p \frac{\partial \psi}{\partial t} = \lambda \frac{\partial^2 \psi}{\partial x^2} + \lambda \frac{\partial^2 \psi}{\partial z^2} + \frac{\partial P_\alpha}{\partial t}\frac{\partial L}{\partial T}\psi + \frac{\partial(\rho H)}{\partial T}\frac{\partial \psi}{\partial t} + \sum_i \delta(x - x_i)\delta(z - z_i)[T(x, z, t; S) - Y_i] \tag{12}$$

$$\psi = 0 \quad t = t_f, \quad 0 < x < x_{\max}, \quad 0 < z < z_{\max} \tag{13}$$

$$\frac{\partial \Psi}{\partial x} = 0 \quad x = 0, \quad 0 < t < t_f, \quad 0 < z < z_{\max} \tag{14}$$

$$-\lambda \frac{\partial \psi(x = x_{\max}, z, t)}{\partial x} = 4\varepsilon\sigma T^3 \psi(x = x_{\max}, z, t) \quad x = x_{\max}, \quad 0 < t < t_f, \quad 0 < z < z_{\max} \tag{15}$$

$$-\lambda \frac{\partial \psi(x, z = 0, t)}{\partial z} = 4\varepsilon\sigma T^3 \psi(x, z = 0, t) \quad z = 0, \quad 0 < t < t_f, \quad 0 < x < x_{\max} \tag{16}$$

$$-\lambda \frac{\partial \psi(x, z = z_{\max}, t)}{\partial z} = 4\varepsilon\sigma T^3 \psi(x, z = z_{\max}, t) \quad z = z_{\max}, \quad 0 < t < t_f, \quad 0 < x < x_{\max} \tag{17}$$

The descent parameter of γ^n is computed as follows:

$$\gamma^n = -\frac{\sum_{j=1}^{N} \int_0^{t_f} [T(x_j, z_j, t) - Y_j(t)]\theta(x_j, z_j, t)\mathrm{d}t}{\sum_{j=1}^{N} \int_0^{t_f} \theta^2(x_j, z_j, t)\mathrm{d}t} \tag{18}$$

where $\theta(x, z, t)$ is the solution of the direct problem in variations [15].

$$\frac{\partial(C\theta)}{\partial y} = \frac{\partial^2}{\partial x^2}(\lambda\theta) + \frac{\partial^2}{\partial z^2}(\lambda\theta) + \frac{\partial P_\alpha}{\partial t}\frac{\partial L}{\partial T}\theta - \frac{\partial}{\partial t}\left[\frac{\partial(\rho H)}{\partial T}\theta\right] + \delta S \tag{19}$$

$$\theta = 0 \quad t = 0, \quad 0 < x < x_{\max}, \quad 0 < z < z_{\max} \tag{20}$$

$$\frac{\partial \theta}{\partial x} = 0 \quad x = 0, \quad 0 < t < t_f, \quad 0 < z < z_{\max} \tag{21}$$

$$-\frac{\partial}{\partial z}(\lambda\theta(x, z = z_{\max}, t)) = 4\varepsilon\sigma T^3 \theta(x, z = z_{\max}, t) \quad z = z_{\max}, \quad 0 < t < t_f, \quad 0 < x < x_{\max} \tag{22}$$

$$-\frac{\partial}{\partial x}(\lambda\theta(x = x_{\max}, z, t)) = 4\varepsilon\sigma T^3 \theta(x = x_{\max}, z, t) \quad x = x_{\max}, \quad 0 < t < t_f, \quad 0 < z < z_{\max} \tag{23}$$

$$-\frac{\partial}{\partial z}(\lambda\theta(x, z = 0, t)) = 4\varepsilon\sigma T^3 \theta(x, z = 0, t) \quad z = 0, \quad 0 < t < t_f, \quad 0 < x < x_{\max} \tag{24}$$

where $\delta S(x, z, t) = D^n(x, z, t)$.

The variation problem is obtained with a variation δS of the source term $S(x, z, t)$. In that case, the temperature $T(x, z, t)$ is perturbed by a variation $\theta(x, z, t)$. Writing equations (1)–(5) for the perturbed solution and subtracting the same equations for the solution T, we obtain the variation problem. For example:

$$\delta\left[\varepsilon\sigma\left(T^4 - T_{\text{inf}}^4\right)\right] = \varepsilon\sigma\left[(T+\theta)^4 - T_{\text{inf}}^4\right] - \varepsilon\sigma\left[T^4 - T_{\text{inf}}^4\right] = \varepsilon\sigma\left[(T+\theta)^4 - T^4\right]$$
$$= \varepsilon\sigma\left[T^4 + 4T^3\theta + O(\theta^2) - T^4\right] = 4\varepsilon\sigma T^3\theta \tag{25}$$

The three systems (direct, in variation and adjoint) are solved numerically using an implicit finite difference method.

3.2. *Regularization*

The inverse problems are ill-posed and numerical solutions depend on the fluctuations occurring at the measurements. Small fluctuations at the measurements can generate big errors in the inverse problem solution. So regularization is needed to stabilize the solution. According to the iterative regularization method, the regularizing discrepancy criterion is used for the stabilization. In fact, the goal is not only the decrease of the residual functional, but also is to obtain the following equality:

$$J(S) \cong \delta^2 \tag{26}$$

where

$$\delta^2 = \int_0^{t_f} \sum_{j=1}^{N} \sigma^2(x_j, z_j, t)\mathrm{d}t \tag{27}$$

$\sigma^2(x_j,\ z_j,\ t)$ is the SD of the temperature measurement errors. The index n^* is the regularization parameter in the method.

4. Numerical simulation

To verify the numerical algorithm, two test cases with exact forms of the source term given *a priori* are analysed. The results of these theoretical estimations are shown in the previous works [15,21]. Here, we present only the results for the second form, a Gaussian source which corresponds to several studies carried out in the laboratory LET2E [15,16]:

$$S(x, z, t) = \frac{8\eta U I_b}{\pi\Phi^2}\ \exp\left(-\frac{8(x^2 + (Vt - y_s)^2)}{\Phi^2}\right)\quad f(z, h)$$
$$\text{with } f(z, h) = \frac{2}{h}\left(1 - \frac{z}{h}\right) \tag{28}$$

where the parameters are: efficiency coefficient $\eta = 0.9$, voltage: $U = 60\,\text{kV}$, current: $I_b = 0.29\,\text{A}$, velocity: $V = 2.5\,\text{mm s}^{-1}$, penetration: $h = 7.1\,\text{cm}$, beam diameter: $\Phi = 0.6\,\text{mm}$. It is well-known that, as formulated, the problem (1)–(6) does not have an unique solution, for e.g., we can easily add to the temperature T, an arbitrary function which satisfies (3)–(6) but not necessarily satisfies (1) and (2). In order to ensure the uniqueness of the solution of the inverse problem given by

equations (1)–(6) one also need to assume a special class of separable heat sources, e.g., $S(x, z, t) = f\_\{1\}(x)f\_\{2\}(z)f\_\{3\}(t)$, as in (28). An excellent research which deals with the uniqueness of the heat source in this class of separable functions is given in [22] and the references therein. The mathematical question of the uniqueness of the solution of the inverse problem (1)–(6) is beyond the scope of our article, and, in fact, our numerical investigations will highlight actually the nonunique features of the solution.

The Gaussian source is divided in two parts. The first one S_v (most energetic part) (figures 6 and 7) is applied in the domain where it goes inside the material (creation of

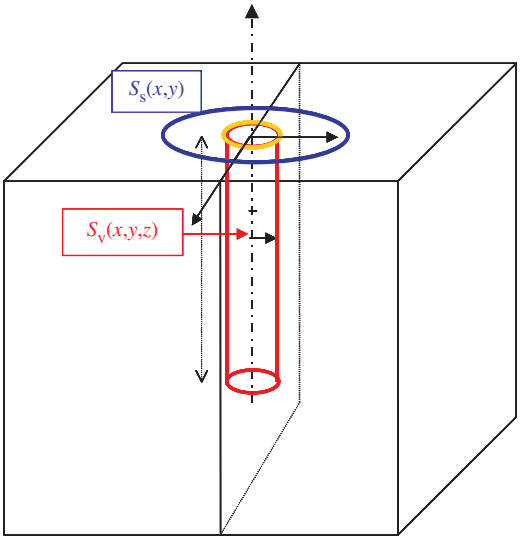

Figure 6. Source definition.

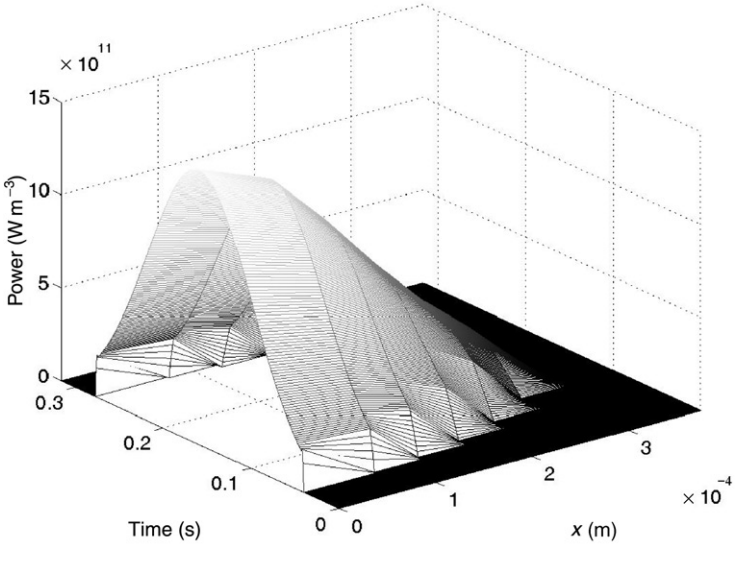

Figure 7. Exact Gaussian source at $z = 0$.

the keyhole). The second one S_s (a ring shape – figure 6) is only a surface heat source corresponding to the "nonactive" part of the beam. In this article, we deal only with the estimation of the most energetic part. With these distributions, we can obtain simulated fused and heat affected zones close enough to those shown in figure 2 [15].

Here, we use, for the estimation, only the exact measurements computed in the HAZ during 0.5 s. This time corresponds to the crossing of the analysed plane by the beam ($0 < t < 0.35$ s) and the beginning of the cooling. Figure 8 shows three computed temperature histories taken in the HAZ. The maximum temperature is around 1400°C. On the welding axis the maximum calculated temperature is around 6000°C, which demonstrates the high damping in the material. In this case, the Fourier number is calculated with average values: $a = 5 \times 10^{-6}\,\mathrm{m^2\,s^{-1}}$, $\Delta x = 1.5$ mm, $\Delta t = 0.001$ s and it is equal to $\Delta F_0 = 0.002$.

The analysis of the estimation results (figures 8–11) permits to underscore the following points. If we compare the exact and estimated temperatures, it can be seen that the results are good enough. But after 200 iterations (figure 9), we do not correctly find the Gaussian shape of the source term in transversal direction (figure 10). Globally, we find the average values of the source. On the other hand, the Gaussian form, as a function of time, is correct. An analysis of this mean heat distribution depending on the depth shows that the estimated form follows well the exact function $f(z, h) = 2/h(1 - (z/h))$.

Another comparison point is the boundary of the fusion zone. Figure 11 shows these exact and estimated boundaries. In the scale of the computational finite difference grid, the shape is followed well. Finally, one can see that it is more difficult to obtain the convergence to the exact source term for the beginning of the welding process. This difficulty comes from the fact that there is no conduction effect forward to the beam (only a transversal plan is analysed). So, the temperature variation is very abrupt when the beam arrives at the study plan. In reality, the thermocouples give information on the beam due to the conduction effects and it is easier to estimate the source term at the beginning of the welding process.

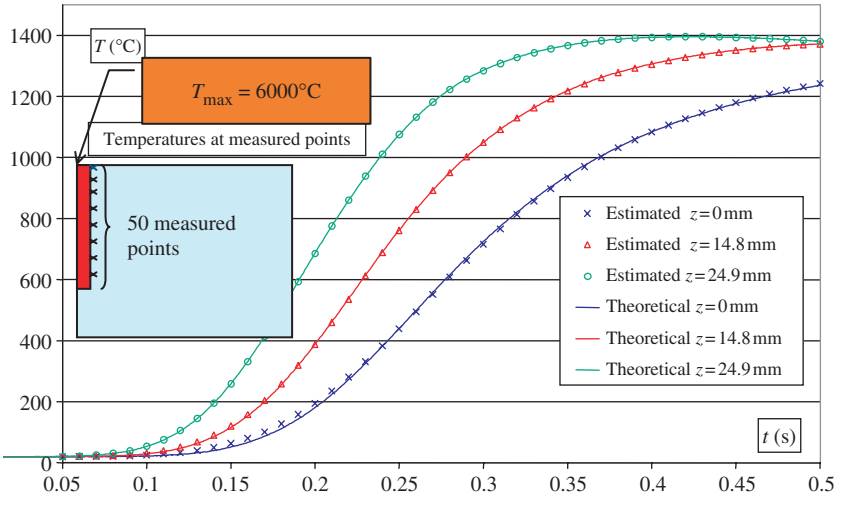

Figure 8. Comparison of the temperatures.

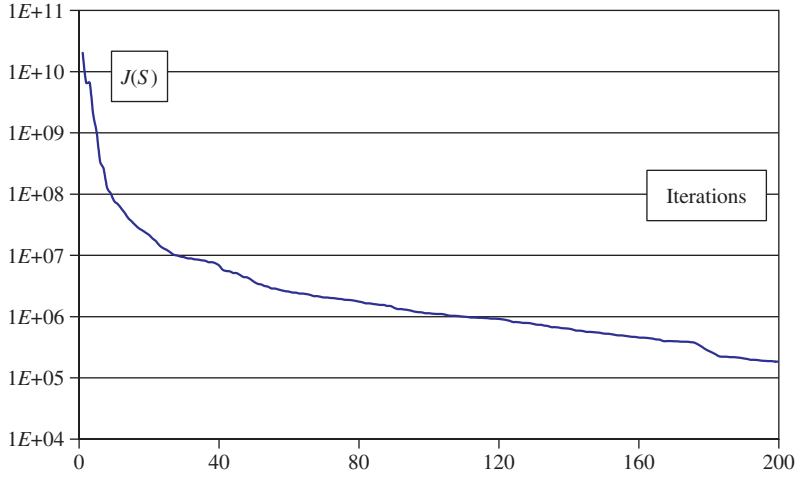

Figure 9. The residual functional evolution.

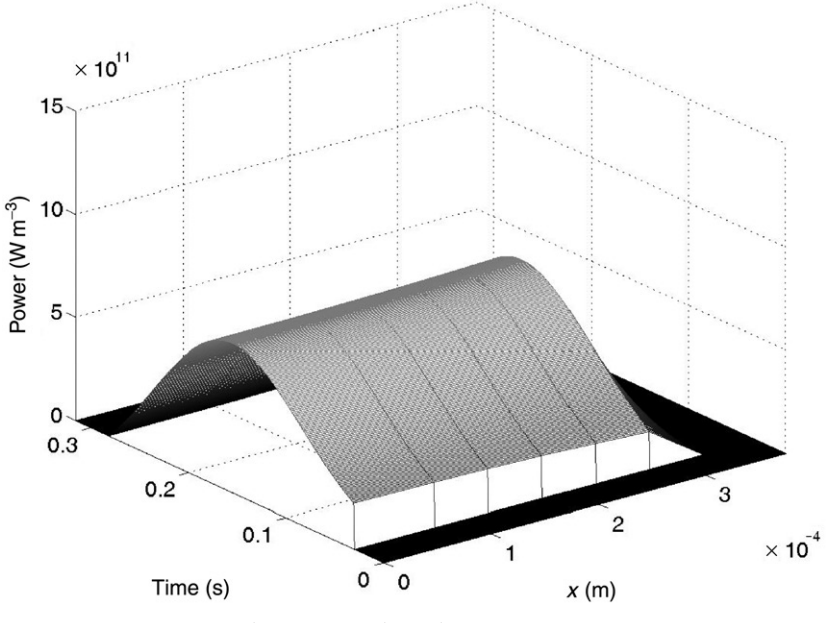

Figure 10. Estimated source at $z = 0$.

5. Application

5.1. *The experiment*

The numerical estimation of the source term (test cases) by different methods [15] has shown that it is difficult to obtain the space distribution of energy in each plane perpendicular to the welding axis. On the other hand, the distribution of energy

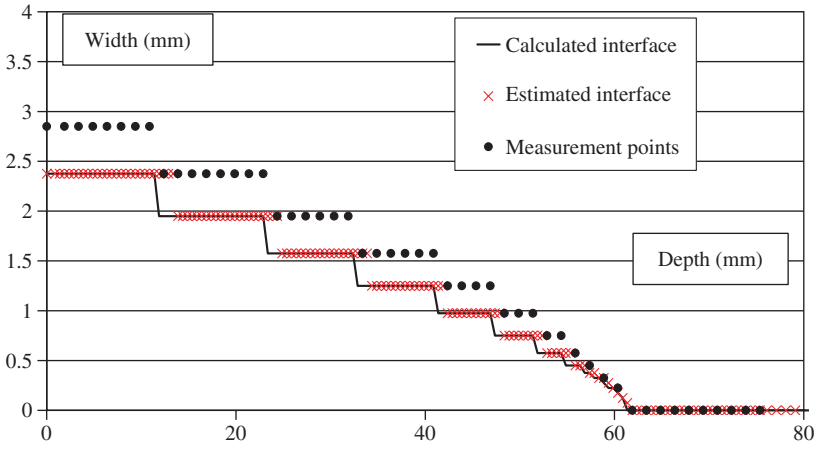

Figure 11. Evolution of the fused zone.

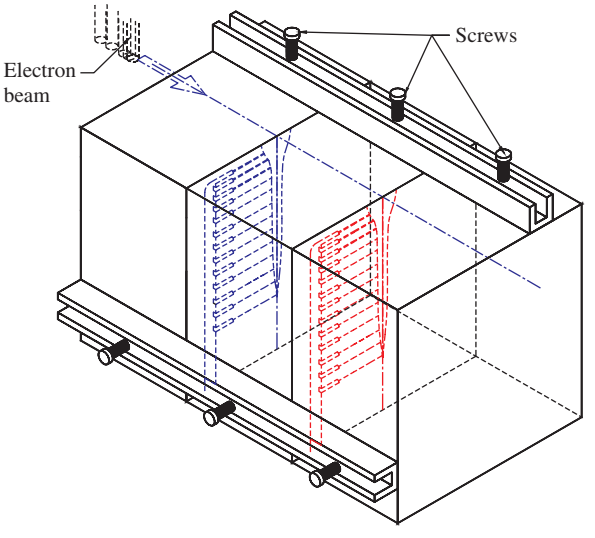

Figure 12. First block.

according to the depth as well as the relative position of the source with respect to this depth remain potentially identifiable. The presented experimental work was carried out in the laboratory LET2E since 2000 [23]. This led us to propose a method of thermocouple installation based on the cutting of the samples in order to carry out a fine instrumentation inside the samples [15,23]. Figure 12 presents the principle of cutting of the samples.

First of all, with the temperature level reached in the molten zone and with the choice of the type of thermocouple (type K – 5 µm), we sought to locate on the macrography (figure 2) the isotherm 1300°C using the direct model. The thermocouples were thus positioned around this isotherm 1300°C ± 0.3 mm. Figure 13 presents the positions retained for the thermocouples. On this figure, we see appearing four interfaces. For practical reasons, we choose to carry out two samples of three blocks having two

interfaces equipped with thermocouples. The R interface (R:n°4) (23 thermocouples) and the B interface (B:n°1) (24 thermocouples) on the first sample (figure 12) and the N interface (N:n°3) (23 thermocouples) and the V interface (V:n°2) (23 thermocouples) on the second sample.

Figure 14 shows the principle of the instrumentation. The sensors were located mainly in the heat affected zones. Each thermocouple is welded by capacitive discharge at the bottom of a small hole (diameter 400 µm, depth 500 µm). The wires of 50 µm diameter are then brought out, thanks to grooves obtained by electroerosion to a basin (with ~20 mm of the axis of welding) where a connection with wires of 125 µm is carried out. The wires are then protected and insulated electrically by a high temperature adhesive (Aremco Ceramabond 571 – $T_{max} = 1750°C$) and by an

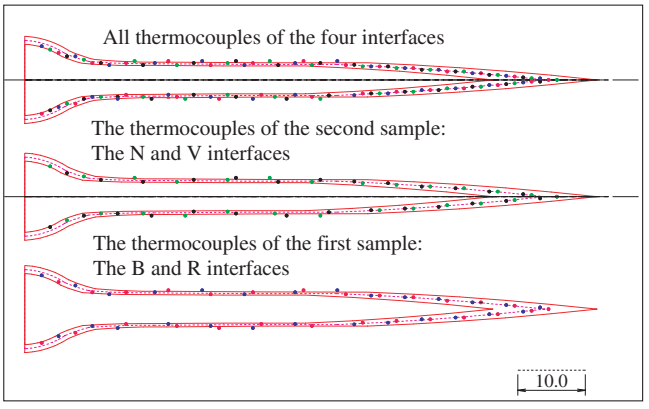

Figure 13. The four interfaces.

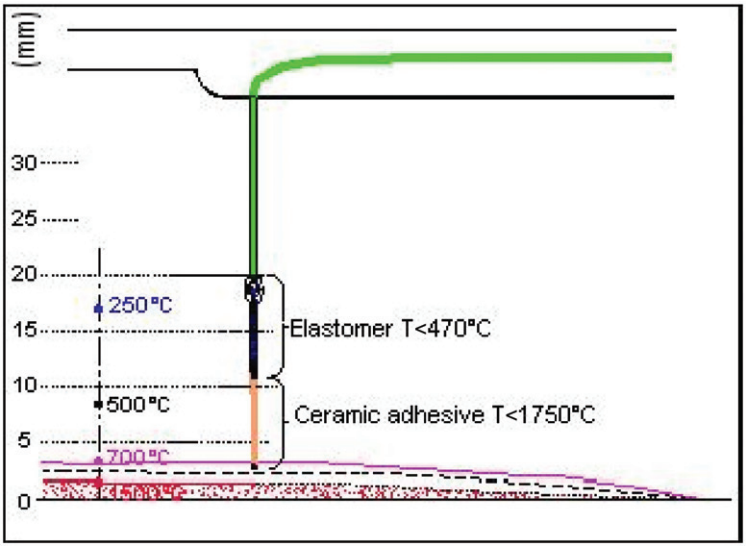

Figure 14. Thermocouple installation.

elastomer ($T < 470°C$). After the thermocouple installation, the recombining of the blocks (figure 12) is obtained by fastening thanks to some welding points.

The EB welding experiment was developed on the industrial site of the DCN establishment. The EB welding machine has a power of 100 kW with a vacuum chamber volume of 800 m^3. An "ARATA" type test [24] was carried out on a strip iron stainless to ensure the reproducibility of the beam form with the shooting reference parameters of welding ($U = 60$ kV, $I_b = 0.29$ A, $I_f = 2.46$ A, $V = 2.5$ mm s^{-1}, distance of shooting = 160 mm). Indeed, the geometry of the beam can change according to the installation ageing. Lastly, the frequency of acquisition is chosen to be 100 Hz over a total recording time of 5 min. With the two samples, we have collected 93 thermal cycles, 52 thermocouples gave very clean recordings which can then be used directly in the estimation code, 28 thermocouples gave truncated information and 13 thermocouples exceeded the acceptable temperature range given by a K type sensor. Figure 15 shows an example of truncated recording.

The last stage of this experimental work consists in an accurate check of the thermocouple locations which is essential to estimate accurately the source term and in a synchronization of the measurements taken on the four interfaces [15]. For this reason, we cut out then rectified the samples to appear the thermocouples (figure 16).

In order to define the exact position of the points of measurements, we worked under binocular provided with a camera and a computer on which a software enabled us to make statements of dimensions (figure 17):

$$x_{\text{real}} = \frac{a+b}{2}(\pm 0.2\,\text{mm}) \tag{29}$$

5.2. *The estimation*

The estimation of the source term is based on 52 temperature profiles obtained on the four interfaces after a temporal retiming. The significant number of the measurement

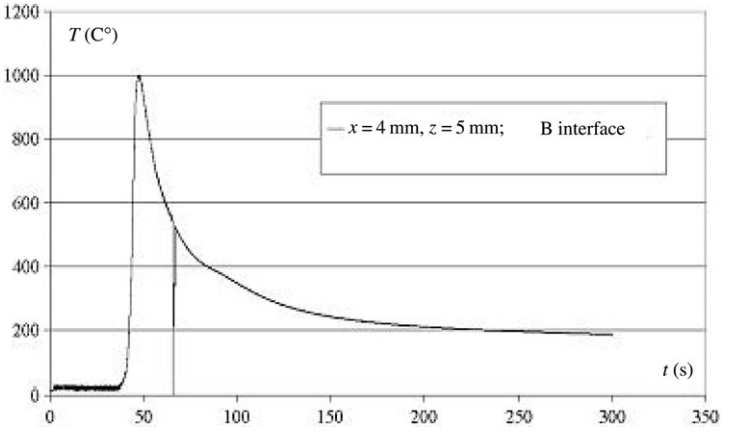

Figure 15. A truncated recording.

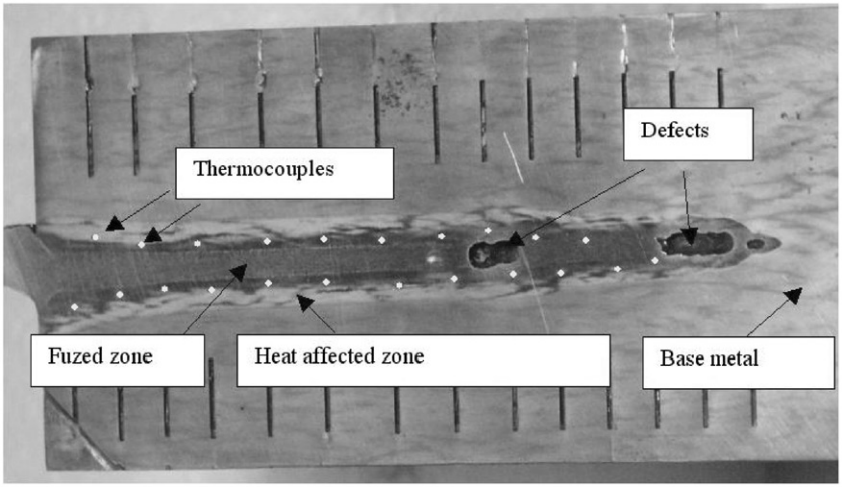

Figure 16. The rectified interface.

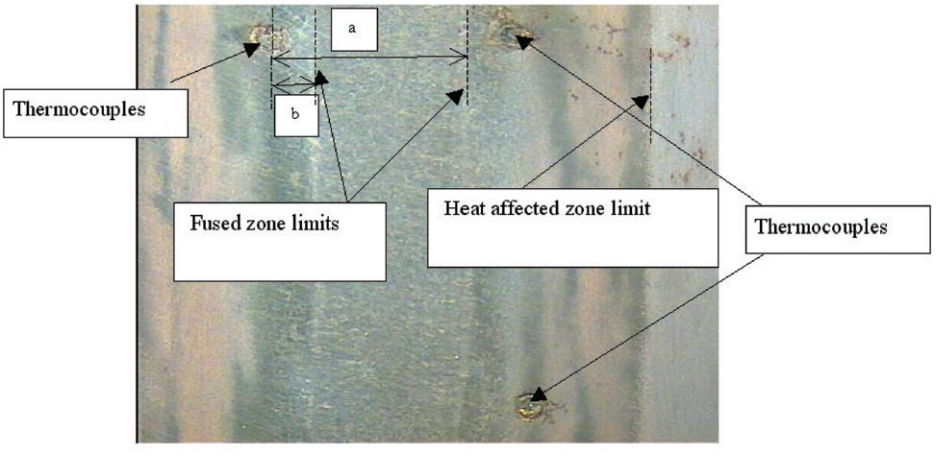

Figure 17. Measurement positions of the thermocouples.

points as a private individual in the vicinity of surface enables us to make some remarks. First of all, calculation was carried out up to 300 iterations.

Figure 18 presents the functional evolution during calculation. In a way identical to the theoretical cases [15], it is shown that the decrease is very fast in the first 20 iterations at the time of convergence towards the density of dissipated power. Thereafter, we note a slower variation after a hundred iterations. At this iteration stage, the estimated source evolves very slowly. The forms of source obtained enable us to note that: first, it is impossible to obtain a correct distribution according to the transverse direction (an average value is obtained), second, the distribution according to time follows a law of the Gaussian type except close to the surface (figure 19) where it appears a quantity of considerable energy to the back of the beam certainly related to the fused metal rejection.

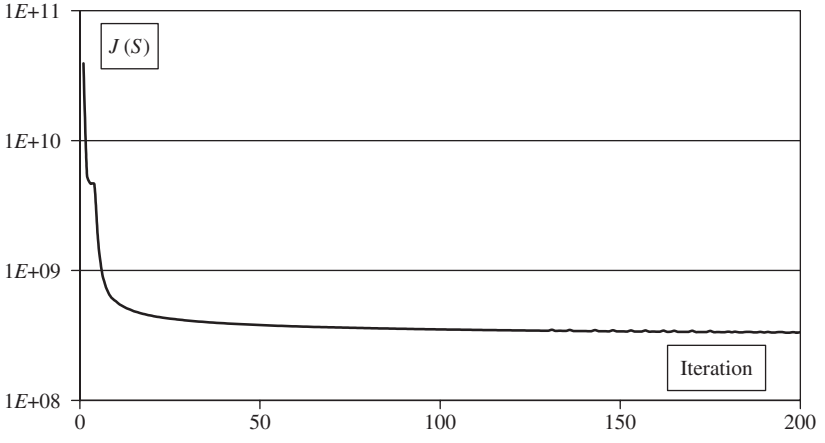

Figure 18. Functional residual.

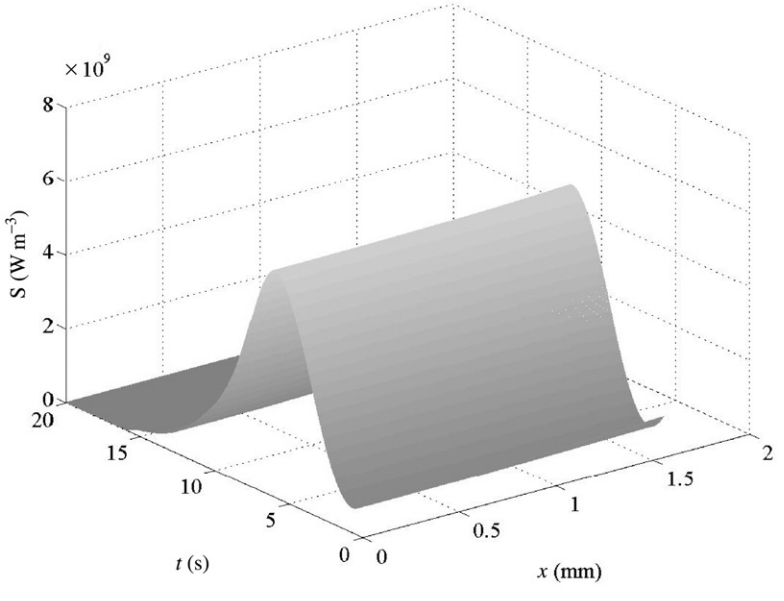

Figure 19. Estimated source at $z = 2.47$ mm.

Moreover, in figure 20, we can note that the distribution of energy is a depth function with first of all an energy zone near to the surface, then an average value on a middle part of the welding, and finally an attenuation of the values to the root of the welding. With the exit of the preceding estimates, we decided to correct the source term in the transverse direction and to impose a Gaussian form. Indeed, for lack of constraint, the method of iterative regularization leads to a spreading out of energy in this direction which does not make it possible to obtain the correct limits of the fused and heat

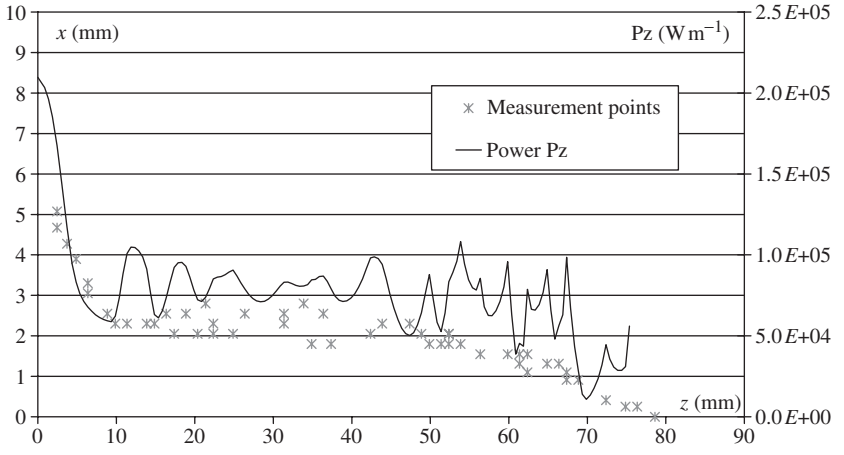

Figure 20. Power density.

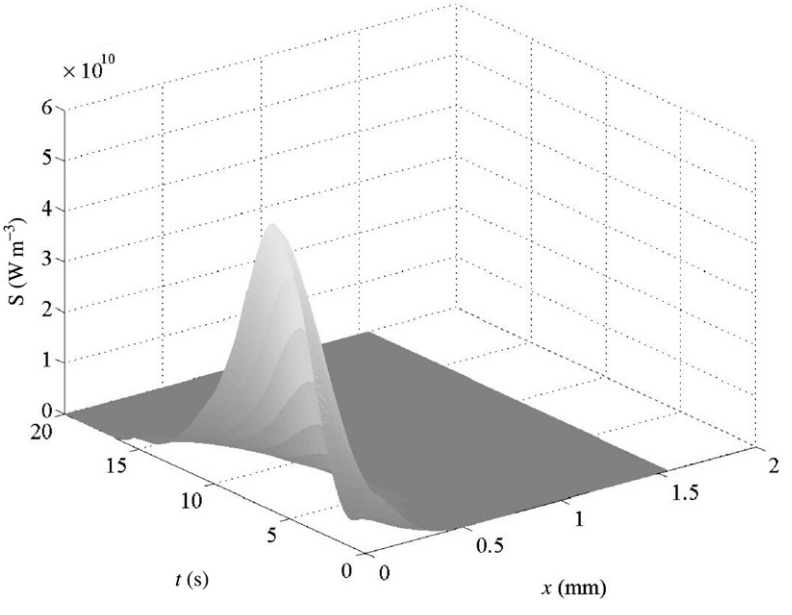

Figure 21. Optimal source at $z = 2.47$ mm.

affected zones compared to the experiment. Figure 21 presents the new form of source obtained starting from the estimated source of figure 19.

6. Conclusions

The objective of this work was to estimate by the iterative regularization method a source term in the case of the EB welding process. A transient thermometallurgic modeling being based on a transverse plan 2D was carried out. The results show that

we have no possibility to correctly describe the energy distribution in the transverse direction. An average and constant value is obtained according to this direction. On the other hand, the distributions according to the direction of welding (y or t) and the depth (z) give us relevant indications. Moreover, the analysis of the energy integral according to depth z shows that the energy distribution is uniform for depths $8 < z < 65$ mm and that it varies at the head and foot of the weld. In the foot of the weld, the power density attenuates while at the head of the weld, the matter rejection accentuates this density. Finally, in order to propose a form of optimal source, and in order to circumvent the difficulty related to the transverse distribution of the energy, we proposed to distribute the average energy estimated in the transverse direction in a Gaussian form. A final analysis of the forms of the fused and heat affected zones shows a difficulty in finding the limit of the fused zone. On the other hand, the limit of the heat-affected zone is very well found.

Nomenclature

a = thermal diffusivity ($m^2 s^{-1}$)
b = constant of the austenite – martensite transformation
C_p, C_γ, C_α = specific heat ($J kg^{-1} K^{-1}$)
D^n = vector of descent direction
dT/dt = variation of the temperature with time ($K s^{-1}$)
$f(\partial T/\partial t)$ = function of the cooling or warming speed
$\Delta F_0 = (a\,\Delta t/(\Delta x)^2)$ = delta Fourier number
h = penetration (m)
H = Enthalpy ($J m^{-3}$)
$\Delta H_{fus}, \Delta H_{vap}$ = enthalpies of the phase change ($J kg^{-1}$)
I, I_f = current and focus current (A)
$J(S)$ = residual functional
∇J^n = the gradient of the residual functional
$L_{\alpha\gamma}$ = heat transformation of phase α to γ ($J m^{-3}$)
M_s = martensite start temperature
n, n^* = iteration number, last iteration
P, P_{eq} = proportion of metallurgic phase (per volume fraction)
P_{max} = maximum proportion of the austenite phase during the austenite – martensite transformation
P_α, P_γ = proportion of the ferrite and austenite phase
$S^{n+1}, S(x, z, t)$ = source term
T_{inf} = external temperature (°C).
T, T_0 = temperature in the sample and initial temperature in the sample (°C)
t = time coordinate (s)
U = voltage (V)
V = velocity ($m s^{-1}$)
x, y, z = spatial coordinates (m)
Y, Y_i, Y_e = experimental temperatures (°C)
γ^n = descent parameter
δ^2 = convergence criterion

ε = emissivity of the sample
ε_1 = arrest criterion
η = efficiency coefficient
$\lambda, \lambda_\alpha, \lambda_\gamma$ = conductivity ($\mathrm{W\,m^{-1}\,K^{-1}}$)
$\rho, \rho_\alpha, \rho_\gamma$ = density ($\mathrm{kg\,m^{-3}}$)
σ = Boltzmann constant: $5.67\ 10^{-8}\ \mathrm{Wm^{-2}K^{-4}}$
σ^2 = standard deviation of the temperature measurement errors
τ = time constant
$\theta(z, r, t)$ = temperature variation
Φ = beam diameter (m)
$\psi\ (z, r, t)$ = adjoint variable

Acknowledgment

The authors acknowledge the CESMAN – DCN Indret for the weld joints.

References

[1] Beck, J.V., Blackwell, B. and St Clair, C.R., 1985, *Inverse Heat Conduction Ill Posed Problems* (New York: Wiley).
[2] Alifanov, O.M., Artyukhin, E.A. and Rumyantsev, S.V., 1995, *Extreme Methods for Solving Ill-posed Problems with Applications to Inverse Heat Transfer Problems* (New York: Begell House).
[3] Jarny, Y., Ozisik, M.N. and Bardon, J.P., 1991, A general optimization method using adjoint equation for solving multidimensional inverse heat conduction. *International Journal of Heat Mass Transfer*, **34**, 2911–2919.
[4] Silva Neto, A.J. and Ozisik, M.N., 1992, Two dimensional inverse heat conduction problem of estimating the time-varying strength of a line source. *Journal of Applied Physics*, **71**, 5357–5362.
[5] Le Niliot, C., 1998, The boundary element method for the time varying strength estimation of point heat sources: application to a two-dimensional diffusion system. *Numerical Heat Transfer B*, **33**, 301–321.
[6] Le Niliot, C. and Gallet, P., 1998, Infrared thermography applied to the resolution of inverse heat conduction problems: recovery of heat line sources and boundary conditions. *Revue Generale De Thermique*, **37**, 629–643.
[7] Peneau, S., Humeau, J.P. and Jarny, Y., 1996, Front motion and convective heat flux determination in a phase change process. *Inverse Problems in Engineering*, **4**, 53–91.
[8] Keanini, R. and Desai, N., 1996, Inverse finite element reduced mesh method for predicting multidimensional phase change boundaries and nonlinear solid face heat transfer. *International Journal of Heat and Mass Transfer*, **39**, 1039–1049.
[9] Hsu, Y.F., Rubinsky, B. and Mahin, K., 1986, An inverse finite element method for the analysis of stationary arc welding processes. *Journal of Heat Transfer*, **108**, 734–741.
[10] Ruan, Y. and Zabaras, N., 1991, An inverse finite element technique to determine the change of phase interface location in two dimensional melting problems. *Communication Applied in Numerical Methods*, **7**, 325–338.
[11] Zabaras, N., 1998, Adjoint methods for inverse free convection problems with application to solidification processes. In: J. Borggaard, E. Cliff, S. Schreck and J. Burns (Eds) *Computational Methods for Optimal Design and Control* (*Birkhauser Series in Progress in Systems and Control Theory*), (Boston: Birkhauser), pp. 391–426; *Proceedings of the U.S. Air Force Optimum Design and Control Symposium*, held at Arlington, VA, 30 September–3 October 1997.
[12] Karkhin, V.A., Plochikhine, V.V. and Bergmann, H.W., 2002, Solution of inverse heat conduction problem for determining heat input, weld shape, and grain structure during laser welding. *Science and Technology of Welding and Joining*, **7**, 224–231.
[13] Doan, D.D., Gabriel, F., Jarny, Y. and Le Masson, P., 2005, Simulation of a weld pool interface motion by a variational inequality approach. In: Chakrabarti, S., Hernandez, S. and Brebbia, C.A. (Eds) *Fluid Structure Interaction and Moving Boundary Problems*, (Southampton: WIT press), pp. 671–681.
[14] Costantini, M., 1995, Simulation numérique du soudage par faisceau d'électrons – contribution au développement d'un modèle prédictif de l'apport d'énergie. Thèse de l'université Paris 6.

[15] Guo, J., 2005, Estimation de la distribution énergétique induite par un faisceau d'électrons dans un matériau métallique – Application au cas du soudage d'un acier. Thèse de l'université de Bretagne Sud.
[16] Rogeon, P., Couedel, D., Carron, D., Le Masson, P. and Quemener, J.J., 2001, Numerical simulation of electron beam welding of metals: sensitivity study of a predictive model. In: H. Cerjak and H.K.D.H. Bhadeshia (Eds) *Mathematical Modelling of Weld Phenomena*, Vol. 5 (London: Institute of Materials Communication), pp. 913–943.
[17] Rogeon, P., Carron, D., Le Masson, P., Couedel, D., Quemener, J.J., Bocquet, P., Gauthier, M. and Balladon, P., 1994, Numerical simulation of electron beam welding of metals: influence of prior austenite grain size on HAZ microstructure in a low alloyed steel. *Welding Journal – Research Supplement* (To appear).
[18] Manuel d'utilisation ''sysweld'', 1994, Systus International.
[19] Leblond, J. and Devaux, J., 1984, A new kinetic model for anisothermal metallurgical transformations in steels including effect of austenite grain size. *Acta Metallurgica*, **32**, 137–146.
[20] Koistinen, D.P. and Marburger, R.E., 1959, A general equation prescribing the extent of austenite-martensite transformation in pure iron-carbon alloys and plain carbon steels. *Acta Metallurgica*, **7**, 59.
[21] Guo, J., Le Masson, P., Artioukhine, E., Loulou, T., Rogeon, P., Carin, M., Dumons, M. and Costa, J., 2006, Estimation of a source term in a two dimensional heat transfer problem: application to an electron beam welding. *Inverse Problems in Engineering*, **14**(1), 21–38.
[22] Savateev, E.G., 1995, On problems of determining the source function in a parabolic equation. *Journal of Inverse and Ill-posed Problems*, **3**, 83–102.
[23] Carin, M., Rogeon, P., Carron, D., Le Masson, P. and Couedel, D., 2004, Numerical simulation of electrons beam welding and instrumental technique. *Revue Européenne des Eléments Finis*, **13**, 247–267.
[24] Arata, Y., 1986, Evaluation of beam characteristics by the ab test method *Plasma, Electron and Laser Beam Technology* (Metals Park, Ohio/USA: American Society for Metals), pp. 177–189.